



UNIVERSIDADE ESTADUAL DE CAMPINAS  
SISTEMA DE BIBLIOTECAS DA UNICAMP  
REPOSITÓRIO DA PRODUÇÃO CIENTÍFICA E INTELLECTUAL DA UNICAMP

**Versão do arquivo anexado / Version of attached file:**

Versão do Editor / Published Version

**Mais informações no site da editora / Further information on publisher's website:**

<https://www.researchsquare.com/article/rs-2670724/v1>

**DOI: <https://doi.org/10.21203/rs.3.rs-2670724/v1>**

**Direitos autorais / Publisher's copyright statement:**

©2023 by Research Square Platform. All rights reserved.

DIRETORIA DE TRATAMENTO DA INFORMAÇÃO

Cidade Universitária Zeferino Vaz Barão Geraldo

CEP 13083-970 – Campinas SP

Fone: (19) 3521-6493

<http://www.repositorio.unicamp.br>

# Harmonic and Interharmonic Estimation Based on Re-Sampling and IpDFT Methods

Henrique L. M. Monteiro<sup>1\*</sup>, Luiz F. A. Rodrigues<sup>2</sup>, Danton D. Ferreira<sup>2</sup>, Thales W. Cabral<sup>3</sup>, Mateus O. Mostaro<sup>4</sup>, Felipe M. Dias<sup>5</sup>, Leandro R. M. Silva<sup>4</sup>, Renato A. Ribeiro<sup>4</sup>, Marcelo A. A. Lima<sup>4</sup> and Carlos A. Duque<sup>4</sup>

<sup>1\*</sup>Institute of Science, Technology, and Innovation, Federal University of Lavras, Antônio Carlos Pinheiro de Alcântara, 855 - Jardim Mediterraneé, São Sebastião do Paraíso, 37950-000, MG, Brazil.

<sup>2</sup>Department of Automatic, Federal University of Lavras, Campus Universitário - Aqueça Sol, Lavras, 37200-900, MG, Brazil.

<sup>3</sup>Department of Communications/DECOM, State University of Campinas/UNICAMP, Av. Albert Einstein, 400 - Cidade Universitária, Campinas, 13083-852, SP, Brazil.

<sup>4</sup>Department of Electric Circuits, Federal University of Juiz de Fora, Campus Universitário, Street José Lourenço Kelmer, s/n - São Pedro, Juiz de Fora, 36036-900, MG, Brazil.

<sup>5</sup>Department of Electrical Engineering, Polytechnic School at University of São Paulo, Prof. Luciano Gualberto Avenue, Travessa do Politécnico, São Paulo, 05508-010, SP, Brazil.

\*Corresponding author(s). E-mail(s): [henrique.monteiro@ufla.br](mailto:henrique.monteiro@ufla.br);

Contributing authors: [luiz.rodriques@estudante.ufla.br](mailto:luiz.rodriques@estudante.ufla.br);

[danton@ufla.br](mailto:danton@ufla.br); [thales.wulfert@engenharia.ufjf.br](mailto:thales.wulfert@engenharia.ufjf.br);

[mateus.mostaro@engenharia.ufjf.br](mailto:mateus.mostaro@engenharia.ufjf.br);

[felipe.dias@engenharia.ufjf.br](mailto:felipe.dias@engenharia.ufjf.br); [leandro.manso@engenharia.ufjf.br](mailto:leandro.manso@engenharia.ufjf.br);

[renato.ribeiro@engenharia.ufjf.br](mailto:renato.ribeiro@engenharia.ufjf.br);

[marcelo.lima@engenharia.ufjf.br](mailto:marcelo.lima@engenharia.ufjf.br);

[carlos,duque@engenharia.ufjf.br](mailto:carlos,duque@engenharia.ufjf.br);

### Abstract

Harmonic and interharmonic estimation is essential for Power System monitoring, particularly for Power Quality (PQ) analysis. These components can interfere with the device functionality, leading to motor heating and energy consumption inefficiency. Usually, the estimation of these components is performed by Fourier Transform; however, the estimation accuracy can decrease in specific scenarios. If the sampled signal is asynchronous or is composed of interharmonics, for example, the energy is spread along the frequency spectrum, causing estimation errors. In this context, this work proposes an innovative method to estimate the harmonic and interharmonic, combining a re-sampling method, based on B-spline with a pre-filter, and Interpolated Discrete Fourier Transform (IpDFT) to avoid the leakage caused by asynchronous sampling and interharmonics. Three real-time re-sampling methods combined with IpDFT are analyzed via simulated voltage signals. The results show that the proposed method is accurate, and robust for all scenarios.

**Keywords:** B-spline, IpDFT, Harmonic, interharmonic, Re-sampling

## 1 Introduction

The Electric Power System (EPS) has become ever more complex due, mainly, to the insertion of non-linear loads, such as cycloconverters, arc furnaces, and Distributed Generation (DG) [1–3]. Thus, Power Quality (PQ) analysis becomes fundamental in order to monitor the distortions present in the network [4]. The waveform distortions occur due to the appearance of signal components different from the fundamental and they are called harmonics and interharmonics, and supra-harmonics, as described in [5–10].

The Discrete Fourier Transform (DFT) algorithm is usually employed to estimate these components due to its low computational complexity [11]. However, although the DFT requires low computational complexity, some aspects related to the leakage and picket-fence effects can be considered to improve the estimation accuracy. These effects can occur when there is an asynchronous sampling and when the DFT resolution is not enough to capture some signal components [12, 13]. Whereas the leakage is caused by the fundamental frequency deviation, the picket-fence is caused by the interharmonics whose frequency is not an integer multiple of the frequency resolution [14–17]. Thus, it demands other methods than DFT to estimate the parameters.

To improve the estimation when there is leakage, the work reported in [18] proposed harmonics and interharmonics groups. However, with asynchronous sampling, the groups are not sufficient. Thus, to improve the accuracy, some parametric and non-parametric methods can be applied to estimate the components more accurately [19–22]. In [20], it is proposed the use of the Estimation of Signal Parameters via Rotational Invariance Technique (ESPRIT), and in [21], the Variational Mode Decomposition (VMD) and Multi interharmonic

Spectrum Separation and Measurement (MSSM) are used to detect and estimate the amplitude and the frequency range of the interharmonics in asynchronous sampling scenarios. The work reported in [22] also employed the MSSM to estimate the interharmonic close to harmonics. Besides these methods having achieved good accuracies in estimating harmonics and interharmonics, they resemble by requiring high computational complexity in the operational phase.

On the other hand, the methods based in the Interpolated Discrete Fourier Transform (IpDFT) [23–27] have been highlighted by presenting low computational complexity. These methods estimate the magnitude and phase of each interharmonic with high accuracy when there is no frequency deviation.

Some works have used re-sampling methods to reduce the effects of leakage due to asynchronous sampling and can improve the frequency components estimation, including high-frequency components with small magnitude. Re-sampling methods such as B-spline and Lagrange are presented in [28–31] and can be applied in EPS signals to estimate frequency components with noise and frequency variation.

In [32], it was shown that the combination of a re-sampling method, based on the Lagrange function, with the IpDFT is an interesting strategy to estimate the harmonics and interharmonics components for frequency deviation scenarios and noisy signals. Although this method presents accurate results, the analysis is made until the second harmonic and the re-sampling method was based on the Lagrange function. In [33] is presented a comparison between two re-sampling methods, B-spline and Lagrange, in which the former proved more accurate than Lagrange. The method presents high accuracy in harmonic estimation; however, the groups proposed in the work to estimate interharmonic present low accuracy, mainly, to estimate interharmonic frequency. Thus, this work presented a combination of the re-sampling method based on B-spline with the inverse function pre-filter and the IpDFT to estimate amplitudes and frequency of the harmonic and interharmonic from EPS signals. The proposed method presented a low computational complexity and provided robustness to estimate the signal components in a frequency variation scenario with different Signal Noise Ratio (SNR) values.

This work is organized as follows: In Section 2, the basic concepts of frequency component estimation are presented. In Section 3, the Lagrange and B-spline interpolation methods are shown. The obtained results are presented in Section 4. Finally, Section 5 summarizes the concluding remarks obtained in this work.

## 2 Basic concepts

In this work, the frequency components estimation scenario is considered with a frequency variation and a steady state of the magnitude and phase of each frequency component. The estimation is applied in signals without events

such as sag, swell, transient, flicker, and other PQ disturbances. However, frequency components such as subharmonics, harmonics, and interharmonics are considered. The supraharmonics are considered as a noise signal.

The referred frequency components are defined according to their frequency values along the spectrum. The first component has a frequency equal to zero and is denominated as continuous component. The sub-harmonics are the components with frequency under the fundamental frequency, and the fundamental frequency is generally equal to 60 or 50 Hz. The harmonic components are the components where the frequency is a multiple of the fundamental frequency, and inter-harmonics are components with higher and non-multiple of the fundamental frequency.

In the following, basic concepts of the frequency components estimation are presented. Firstly, the DFT is presented, showing its performance for a signal with frequency variation and interharmonics.

## 2.1 Discrete Fourier Transform for frequency components analysis

The Discrete Fourier Transform (DFT) is widely used for spectral signal analysis. Considering a signal  $x[n]$  with fundamental frequency  $f_1$  and a sampling frequency  $f_s = (N \cdot f_1)/N_c$ , where  $N_c$  is the number of cycles and  $N$  is the total number of points in  $N_c$  cycles, this signal can be written as

$$\begin{aligned}
 x[n] = & A_0 + \sum_{k=1}^{sh_{max}} A_{sh,k} \cdot \sin \left( 2\pi \frac{f_{sh,k}[n]}{f_s} n + \Phi_{sh,k} \right) \\
 & + \sum_{k=1}^{h_{max}} A_{h,k} \cdot \sin \left( 2\pi k \frac{f_1[n]}{f_s} n + \Phi_{h,k} \right) \\
 & + \sum_{k=1}^{ih_{max}} A_{ih,k} \cdot \sin \left( 2\pi \frac{f_{ih,k}[n]}{f_s} n + \Phi_{ih,k} \right) \\
 & + s[n], -\infty < n < \infty,
 \end{aligned} \tag{1}$$

where  $A_0$  is the zero frequency component,  $k$  is the order of the harmonic and  $n$  correspond to the samples of the signal.  $A_{sh,k}$ ,  $A_{h,k}$  and  $A_{ih,k}$  are the magnitude of the  $k^{th}$  sub-harmonic, harmonic and interharmonic component, respectively.  $f_{sh,k}[n]$  and  $f_{ih,k}[n]$  are the sub-harmonic and interharmonic frequency.  $\phi_{sh,k}$ ,  $\phi_{h,k}$  and  $\phi_{ih,k}$  are the phase of the  $k^{th}$  sub-harmonic, harmonic and interharmonic component.  $sh_{max}$ ,  $h_{max}$ , and  $ih_{max}$  are the maximum sub-harmonic, harmonic, and interharmonic order that is considered in the signal. The signal  $s[n]$  is defined as the noise and supraharmonics.

In practical applications, the signal presented in (1) has a finite length. Thus, a window function  $w[m]$  is applied in  $x[n]$ , resulting in

$$x_w[n] = x[n] \cdot w[m], \quad 0 < m < N, \quad (2)$$

where  $w[m]$  can represent several windows functions applied to signal  $x[n]$ . Some examples of  $w[n]$  functions are rectangular and hanning, in which the rectangular window is more simple to apply in the signals. However, the hanning function can help to avoid leakage.

After applying the window, the DFT can be applied in the  $x_w[n]$ , according to

$$X_w[k] = \sum_{m=0}^N x[m]_w e^{-j2\pi km/N}. \quad (3)$$

When the window is applied, and the signal length is one or more integer cycles of the fundamental component, the sampling process is called synchronous or coherent. Otherwise, the sampling is defined as asynchronous or non-coherent. To avoid the leakage effect, the sampling should be synchronous.

## 2.2 Leakage caused by fundamental frequency variation

As previously reported, if the signal is sampled synchronously, the estimation of the components is more accurate when compared to asynchronous sampling due to a frequency deviation. Figure 1 shows the effect of two sampling modes, synchronous and asynchronous. In Figure 1 (a) and (b), a nominal frequency of 60 Hz is considered for synchronous sampling and 59 Hz for asynchronous sampling. Thus, in Figure 1 (a), the single component with a nonzero energy bin is obtained in the center of the main lobe. In Figure 1 (b), the sampling is asynchronous; therefore, there is leakage due to the frequency deviation.

## 2.3 Leakage caused by the presence of interharmonics

As mentioned earlier, interharmonics are components with frequencies non-integer multiple of the fundamental [34]. Often, these components do not assume integer multiples of the DFT frequency resolution. In the presence of interharmonics, there are two kinds of leakage: Short-range leakage and Long-range leakage [35].

Short-range leakage occurs when there is an interharmonic component located away from the frequency of a harmonic component. Thus, the leakage caused by this interharmonic component can be neglected due to the distance between the frequency components. Figure 2 shows this type of leakage in the frequency domain due to the signal represented by

$$x[n] = \sin(2\pi 60nT_s) + 0.1 \sin(2\pi 117.5nT_s), \quad (4)$$

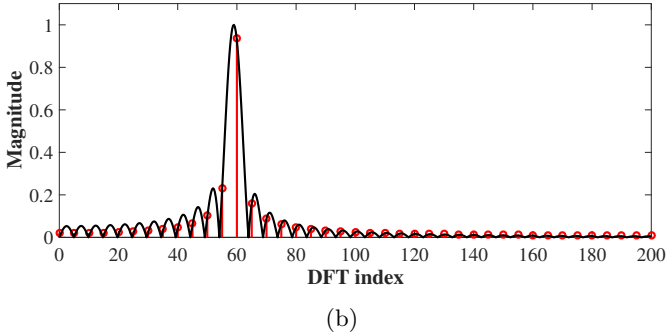
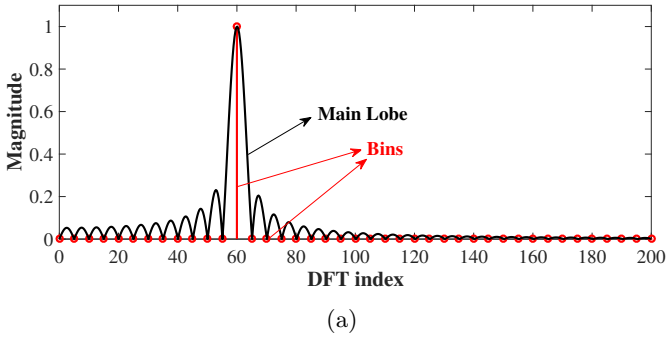


**Figure 1** Frequency domain of a (a) synchronous and (b) asynchronous sampling.

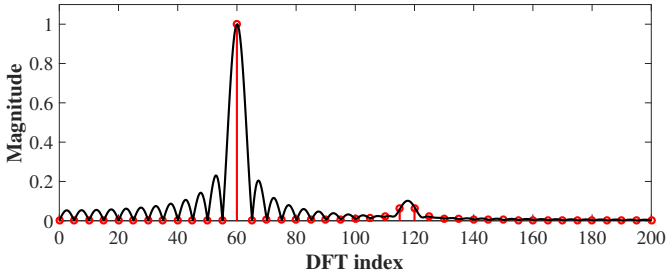


**Figure 2** Short Range Leakage.

considering a window with 12 cycles of the fundamental frequency. In this case, the frequency resolution is 5 Hz.

In Figure 2, the spreading effect is around 120 Hz due to the presence of an interharmonic located at 117.5 Hz. For a better result, the frequency resolution must assume a value so that the interharmonic frequency is an integer multiple of the frequency resolution. In this case, due to interharmonic distance, the harmonic amplitude is not affected.

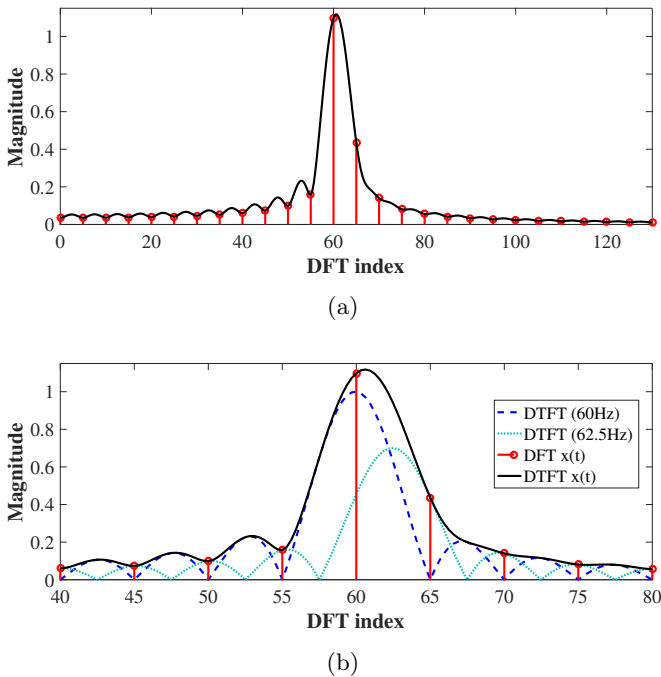


**Figure 3** Long Range Leakage. (a) DTFT and DFT of signal  $x[n]$  and, (b) representation of the two DTFT frequency components overlapping.

Long-Range Leakage occurs due to interference between the Discrete Time Fourier Transform (DTFT) of two or more components located close to each other. When an interharmonic is close to a harmonic, spectral interference occurs due to the complex superposition, which is related to harmonic and interharmonic magnitudes and phases [35]. Figure 3 shows this overlap for a signal represented by

$$x[n] = \sin(2\pi 60nT_s) + 0.3 \sin(2\pi 62.5nT_s). \quad (5)$$

Figure 3 (a) and (b) show the leakage occurred due to the interference between the fundamental component and an interharmonic when their frequencies are close.

Some methods can be applied to reduce the leakage or to group the harmonic and interharmonic energy in a single bin. Considering the leakage caused by asynchronous sampling, re-sampling methods can be employed to set an integer number of cycles in a window. However, the re-sampled signal does not avoid the picket-fence effect. Thus, the interharmonic estimation requires an additional method, such as the three-point IpDFT as presented in [18].

In the following, some re-sampling methods and IpDFT. These methods can help to improve the harmonic and interharmonic estimation, reducing or eliminating the leakage caused by asynchronous sampling, and improving the estimation when there is interharmonic leakage.

### 3 Re-sampling

The re-sampling is an important technique that can aid in harmonic and interharmonic estimation if the sampling is asynchronous. The re-sampling removes the leakage, and thus, the estimation errors are mitigated. In this work, two re-sampling methods, using Lagrange and B-spline functions, are compared. In the following, both are described in more detail.

#### 3.1 Lagrange Function

One of the most compact methods for representing polynomials is the Lagrangian form [31], represented by

$$y[m] = \sum_i \left( \prod_{j \neq i} \frac{m - n_j}{n_i - n_j} \right) x[n_i], \quad i, j = 1, 2, \dots, k, \quad (6)$$

where  $m$  is the index of the re-sampled signal  $y[m]$ , and  $i$  and  $j$  are the samples of the signal sampled  $x[n]$ , presented in (1). The Lagrange polynomials can represent any degree, defined by the number of points considered in  $x[n]$  to estimate a unique sample of  $y[m]$ . Thus, considering  $k$  points, the degree polynomial is  $k - 1$ . For example, if  $i, j = 0, 1, 2$ , there is a polynomial of degree two.

The re-sampled process in real-time applies filters to store the samples in a memory, according to the polynomial to be obtained [11]. The values contained in the memory are shifted or discarded when a new  $x[n]$  sample comes in. Figure 4 presents the re-sampling process considering a memory with four positions. The index  $n$  represents the actual sample,  $n - 2$  and  $n - 1$  are past samples, and  $n + 1$  represents a future sample. The distance from the  $x[n]$  sample to the point to be re-sampled is  $\alpha$ , and it is modified according to the estimated fundamental frequency. This process can be defined according to equation (6), which is considered the intervals from  $(n - 2)$  to  $(n + 1)$ . The value of  $\alpha$  is defined by

$$n < \alpha \leq n + 1. \quad (7)$$

The equation (6) can be developed to obtain  $\alpha$  by the following way:

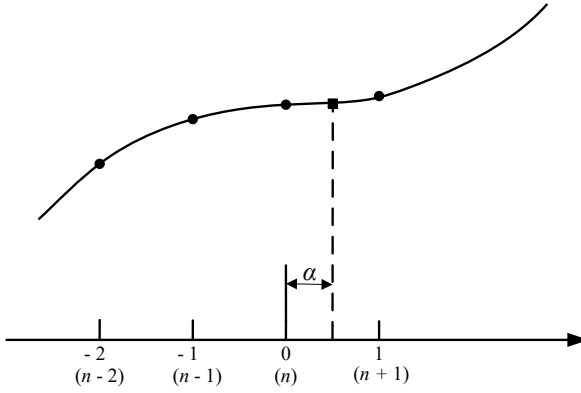


**Figure 4** Representation of the re-sampling process.

$$\begin{aligned}
 y[m] = & \frac{\alpha - (n-1)}{(n-2) - (n-1)} \cdot \frac{(\alpha - n)}{(n-2) - n} \cdot \frac{[\alpha - (n+1)]}{(n-2) - (n+1)} \cdot x[n-2] \\
 & + \frac{\alpha - (n-2)}{(n-1) - (n-2)} \cdot \frac{(\alpha - n)}{(n-1) - n} \cdot \frac{\alpha - (n+1)}{(n-1) - (n+1)} \cdot x[n-1] \\
 & + \frac{\alpha - (n-2)}{n - (n-2)} \cdot \frac{\alpha - (n-1)}{n - (n-1)} \cdot \frac{\alpha - (n+1)}{n - (n+1)} \cdot x[n] \\
 & + \frac{\alpha - (n-2)}{(n+1) - (n-2)} \cdot \frac{\alpha - (n-1)}{(n+1) - (n-1)} \cdot \frac{\alpha - n}{(n+1) - n} \cdot x[n+1].
 \end{aligned} \tag{8}$$

Considering  $n$  equal to zero and  $\alpha$  in the interval  $0 < \alpha \leq 1$ ,

$$\begin{aligned}
 y[m] = & \alpha^3 \cdot \left( -\frac{1}{6} \cdot x[-2] + \frac{1}{2} \cdot x[-1] - \frac{1}{2} \cdot x[0] + \frac{1}{6} \cdot x[1] \right) \\
 & + \alpha^2 \cdot \left( \frac{1}{2} \cdot x[-1] - x[0] + \frac{1}{2} \cdot x[1] \right) \\
 & + \alpha \cdot \left( -\frac{1}{6} \cdot x[-2] - x[-1] + \frac{1}{2} \cdot x[0] + \frac{1}{3} \cdot x[1] \right) \\
 & + x[0].
 \end{aligned} \tag{9}$$

Applying the Z transform in (9),  $y[m]$  can be represented by:

$$Y(z) = (H_0(z)\alpha^3 + H_1(z)\alpha^2 + H_2(z)\alpha + H_3(z)) \cdot X(z). \tag{10}$$

where  $H_0(z)$ ,  $H_1(z)$ ,  $H_2(z)$  and  $H_3(z)$  is defined by

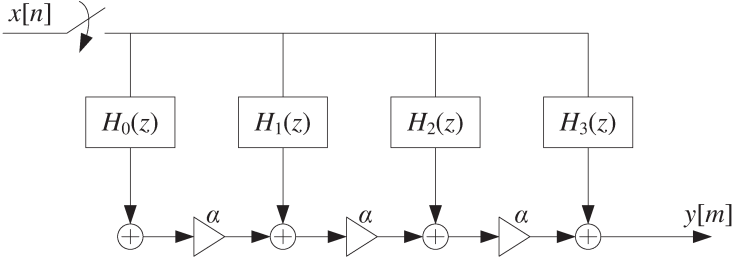


**Figure 5** Farrow Structure of the 3rd order.

$$\begin{aligned}
 H_0(z) &= -\frac{1}{6} \cdot z^{-2} + \frac{1}{2} \cdot z^{-1} - \frac{1}{2} + \frac{1}{6} \cdot z \\
 H_1(z) &= \frac{1}{2} \cdot z^{-1} - 1 + \frac{1}{2} \cdot z \\
 H_2(z) &= \frac{1}{6} \cdot z^{-2} - z^{-1} + \frac{1}{2} + \frac{1}{3} \cdot z \\
 H_3(z) &= 1.
 \end{aligned} \tag{11}$$

The equation (10) presents a filter structure that is represented in Figure 5. In this structure, a multiplier,  $\alpha$ , is inserted before each summation, featuring a time-varying filter. If  $\alpha$  is zero, the sample  $y[m]$  is equal to  $x[n]$  due  $H_3(z)$  to be 1. Note that the indexes of the signals  $x[n]$  and  $y[m]$  are different. These indexes differ due to the re-sampling process. In this process, the interval between two samples can be considered more than once or can be disregarded depending on the fundamental frequency. To implement the re-sampling in real-time according to the filter structure, Algorithm 1 is employed. In Algorithm 1,  $T'_s$  is the estimated sampling time, and  $\lambda$  is the ratio between the estimated sampling time and sampling time established in the process ( $T_s$ ). The algorithm initializes, considering the previous values of each parameter. In step two,  $T'_s$  is updated by:

$$T'_s = \frac{1}{(N_{pc} \cdot f_{e1})}, \tag{12}$$

where  $N_{pc}$  is the number of points in each cycle and  $f_{e1}$  is the estimated fundamental frequency of the system. In step three, if the condition is true,  $y[m]$  is estimated by (9), the index  $m$  is updated, and the algorithm returns to step 2. If it is not true, the algorithm goes to step four, the buffer,  $\alpha$ , and  $n$  are updated, and the algorithm goes to step 2 again.

---

**Algorithm 1** - Steps of re-sampling process.

---

**Initialization:**

$$\begin{aligned} T'_s &= T_s \\ \alpha &= 0 \\ m &= 0 \\ n &= 0 \end{aligned}$$

**Update  $T'_s$  and calculate  $\lambda = T'_s/T_s$ :**

$$\alpha = \alpha + \lambda$$

if  $\alpha < 1$ , find  $y[m]$  through equation (9):

$$m = m + 1$$

go to step 2

if  $\alpha \geq 1$ , update the buffer with the new sample and update subtract the value of  $\alpha$

$$\alpha = \alpha - 1$$

$$n = n + 1$$

go to step 2

**end**

---

### 3.2 B-spline

Re-sampling based on B-spline [36] is similar to Lagrange and can also be applied in real-time. The quality of this method is evaluated concerning the smoothing of the curves obtained by the re-sampled signal. However, the samples of the  $y[m]$  can not assume the signal values if the process is not composed by pre-filter. The cubic B-spline, as presented in [37], can be defined as

$$\beta^{(3)}(t) = \begin{cases} \frac{2}{3} - t^2 + \frac{t^3}{2}, & 0 < t < 1 \\ \frac{(2-t)^3}{6}, & 1 \leq t < 2 \\ 0, & 2 \leq t. \end{cases} \quad (13)$$

Thus, re-sampled value of  $y[m]$  can be found applying  $\beta_i^{(3)}$  on the input signal. It leads to

$$y[\alpha] = \sum_{i=-1}^2 \beta_i^{(3)}[\alpha]x[n+i]. \quad (14)$$

This function can be presented as

$$\begin{aligned}
\hat{y}[m] = & x[n-1] \left[ -\frac{\alpha^3}{6} + \frac{\alpha^2}{2} - \frac{\alpha}{2} + \frac{1}{6} \right] \\
& + x[n] \left[ -\frac{\alpha^3}{2} - \alpha^2 + \frac{2}{3} \right] \\
& + x[n+1] \left[ -\frac{\alpha^3}{2} + \frac{\alpha^2}{2} + \frac{\alpha}{2} + \frac{1}{6} \right] \\
& + x[n+2] \left[ -\frac{\alpha^3}{6} \right].
\end{aligned} \tag{15}$$

Note that the parameter  $\alpha$  is the distance between the sample  $x[n+2]$  and the point to be re-sampled of the possible estimated signal in continuous time  $\hat{y}(t)$ . Applying the  $Z$  transform, the following expression can be determined:

$$\begin{aligned}
H_0(z) &= -\frac{1}{6} \cdot z^{-1} + \frac{1}{2} - \frac{1}{2} \cdot z + \frac{1}{6} \cdot z^2 \\
H_1(z) &= \frac{1}{2} \cdot z^{-1} - 1 + \frac{1}{2} \cdot z \\
H_2(z) &= -\frac{1}{2} \cdot z^{-1} + \frac{1}{2}z + \frac{1}{3} \cdot z \\
H_3(z) &= \frac{1}{6}z^{-1} + \frac{2}{3} + \frac{1}{6}z.
\end{aligned} \tag{16}$$

Thus, as can be seen, the structure of the re-sampling using the B-spline functions is similar to re-sampling applying the Lagrange function, as presented in (10). In the re-sampling with B-spline functions, the output signal does not assume the correct values of the original signal samples when the  $\alpha$  is zero. Thus, to improve this process, filters are applied before the re-sampling. Due to these filters being inserted previously, they are defined as pre-filters.

In this work, two different pre-filters are presented, one defined as inverse B-spline function [37] and another defined as least square approximation [28, 30]. In the first, the pre-filter is based on inverse function of  $H_3(z)$ . Thus, when  $\alpha$  is zero,  $y[m]$  receives the sample  $x[n]$ . The  $H_3(z)$  inverse function is defined by:

$$P_f(z) = \frac{6}{z^{-1} + 4 + z}. \tag{17}$$

In [28] is presented a filter obtained by z-transform as follows:

$$h[n] = g \sum_{k=-\infty}^{\infty} \alpha^k \delta[n-k], \tag{18}$$

where  $g = \frac{1}{2\sqrt{3}}$ ,  $\alpha = \sqrt{3} - 2$  and  $\delta[n]$  is the Kronecker delta. However, (18) has infinity coefficients and is a non-causal filter. Based on [28], this work uses a truncated and causal pre-filter that can be applied as:

$$x_1[n] = \alpha \cdot x_1[n - 1] - 6 \sum_{k=-M}^0 \alpha^{k+1} x[n - k], \quad (19)$$

where  $x_1[n]$  is the pre-filter output and  $M$  is the number of coefficients used in pre-filter. In the second B-spline pre-filter, the frequency response of the cubic B-spline function is approximate to an ideal low-pass filter. Considering a sinc function the frequency response can be represented by:

$$p_f(t) = \sum_{n=-\infty}^{\infty} \text{sinc}(t - nT_s)x(nT_s), \quad (20)$$

where the function  $\text{sinc}(t)$  is represented by:

$$\text{sinc}(t) = \begin{cases} \frac{\sin(\pi t)}{\pi t}, & \text{for } t \neq 0 \\ 1, & \text{for } t = 1. \end{cases} \quad (21)$$

The cubic B-spline frequency response is represented by:

$$B(\omega) = \left( \frac{\sin(\omega/2)}{\omega/2} \right)^4. \quad (22)$$

The frequency responses of the ideal approximation and cubic B-spline filters are shown in Figure 6. In order o approximate the output filter to the ideal, we considered the least square approximation as presented in [30]:

$$P_f(\omega) = \frac{B(\omega)}{\sum_i \|B(\omega + 2i\pi)\|^2}, \quad (23)$$

where  $P_f(\omega)$  is the B-spline pre-filter.

Establishing the approximation function, the coefficients of the filter that minimize the difference between the curves of the ideal pre-filter and the pre-filter can be acquired through (23). The implementation differences between the re-sampling process applying Lagrange and B-spline functions occur in the filter coefficients and the pre-filter. The comparison can be seen in (11) and (16).

### 3.3 Interpolated Discrete Fourier Transform

Although resampling eliminates the leakage caused by asynchronous sampling, another method is needed to improve the performance of interharmonic component estimation. Therefore, in this work, the IpDFT method is proposed. This method consists in interpolating the range where there is leakage caused

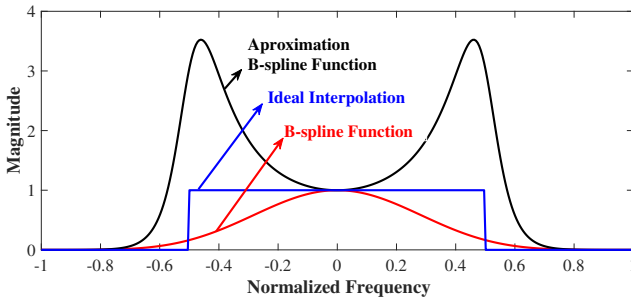


**Figure 6** Frequency responses of the cubic B-spline function, the approximation function, and the ideal response.

by interharmonics with a frequency non-multiple of the resolution to estimate the amplitude and frequency values of each component.

Initially, a threshold is defined in order to establish the range where there are interharmonics (in this work we used a threshold of 3% of the fundamental magnitude). Next, the frequencies of the three largest magnitudes in the range are defined,  $k_0$ ,  $k_1$ , and  $k_2$ , where  $k_1$  is the frequency of the largest value among the three selected. With the values established, we estimate the frequency of the interharmonic by

$$\hat{f}_{ih} = (k_1 + \delta) \frac{f_s}{N} \quad (24)$$

where  $\delta$  is the distance between the frequency of the largest magnitude selected and the interharmonic estimated. The  $\delta$  can be found by

$$\delta = \frac{\|Y[k_0]\| - \|Y[k_2]\|}{\|Y[k_0]\| + 2\|Y[k_1]\| + \|Y[k_2]\|}. \quad (25)$$

Thus, the interharmonic magnitude can be estimated by [18]

$$\hat{A}_{ih} = \|Y[k_1]\| \frac{\pi \delta}{\sin(\pi \delta)} [(\delta)^2 - 1]. \quad (26)$$

Although the IpDFT method has some limitations due to the interference of harmonics, in this work it was considered the resampling process that contributes to a better performance of interharmonic estimation, making the process with high accuracy and low computational complexity.

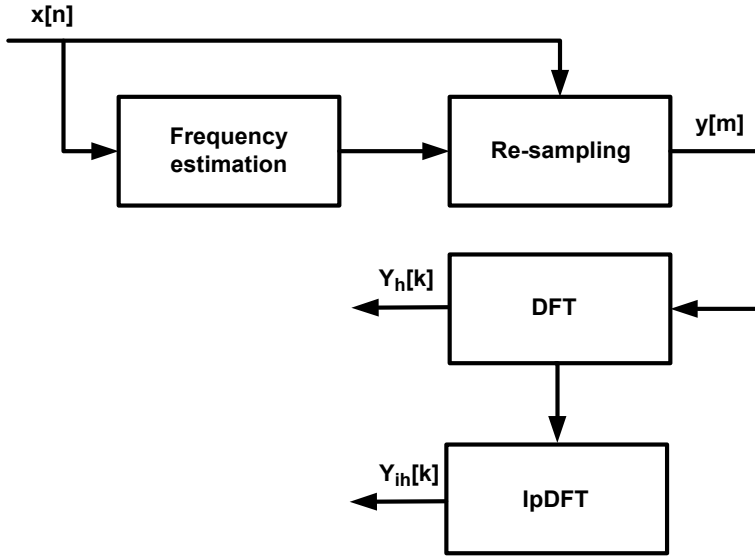
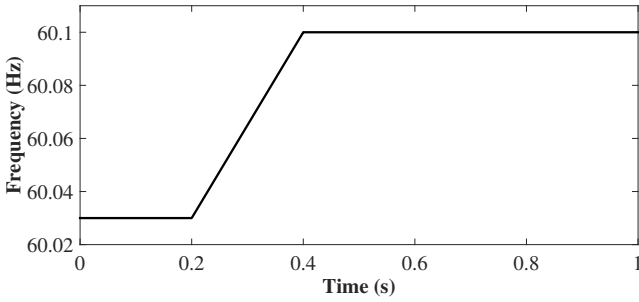


**Figure 7** Representation of the harmonic and interharmonic estimation.

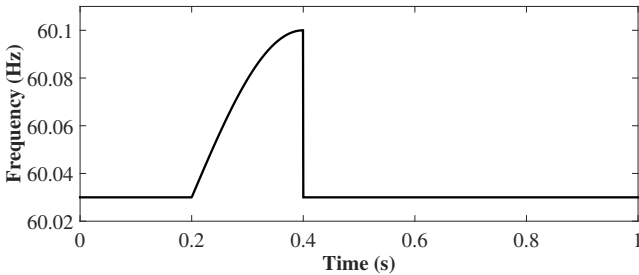
## 4 Results

In this section, a signal with SNR of 45 dB in a 60 Hz system with harmonics of order 1, 3, 7, 11, 13, 15, 19, 21, 27, 31, 37, 45 and 49 is considered. The magnitude of each component is set as  $1/h$ , where  $h$  represents the harmonic order. For the frequency estimation, Phase Locked Loop (PLL) technique is applied as presented in [38]. The window length of the signal is defined with 4,096 samples in 12 cycles of the fundamental frequency. In this work, we considered a Hanning window to be applied in the re-sampled signal. Figure 7 shows the process of harmonic and intrerharmonic estimation. In the first step, the signal  $x[n]$  is submitted to frequency estimation, in which the output is an input of the re-sampling process. In this step, the signal is re-sampled such that  $y[m]$  contains 4,096 samples. After re-sampling, the Hanning window is applied in the signal and the DFT is applied in the  $y[m]$  to obtain the harmonics estimated ( $Y_h[k]$ ). Then, the interharmonics are detected through a threshold and the estimation is processed by the three-point IpDFT ( $Y_{ih}[k]$ ).

In the following, five cases are presented. In the first case, signals with ramp and sinusoidal frequency variation are considered. In the second case, we consider signals composed of interharmonics. In the third case, the signals are considered with a frequency deviation of 0.1 Hz and interharmonics. In the fourth case, the signals are composed of interharmonics and we analyzed the estimation performance for different SNR. In the fifth case, two re-sampling methods based on B-spline are compared. For all cases, the results are obtained considering a mean of 100 signals.



(a)



(b)

**Figure 8** Frequency variation: (a) ramp and (b) sinusoidal.

#### 4.1 Signals with ramp and sinusoidal frequency variation

In this case, the results with frequency variation are considered, as shown in Figure 8 (a) and (b). At first, in Figure 8 (a), the frequency varies in the ramp. Then, a sinusoidal variation is presented in Figure 8 (b). The variation starts in 0.2 s considering a frequency equal to 60.03 Hz and achieves 60.1 Hz in 0.4 s. The estimation of the components is realized in this interval. The relative errors obtained in the harmonic estimation are shown in Figure 9 and Figure 10. Analyzing these errors, we noted that the re-sampling method based on the Lagrange function obtained the highest error. In Table 1 and Table 2 the Mean Relative Error (MRE) and the Mean Square Error (MSE), obtained from the harmonic magnitude estimation are presented. As can be seen, all the methods present satisfactory results, maintaining the value below 0.5%. The largest error is presented by resampling with the Lagrange function and the smallest is obtained by the B-spline based method using the pre-filter with the inverse function.

**Table 1** MRE obtained considering a ramp and sinusoidal variation.

Re-sampling Method	Ramp	Sinusoidal
Lagrange	0.23	0.19
B-spline Inverse F.	0.04	0.04
B-spline least square	0.12	0.10

**Table 2** MSE obtained considering a ramp and sinusoidal variation.

Re-sampling Method	Ramp	Sinusoidal
Lagrange	0.42	0.35
B-spline Inverse F.	0.05	0.06
B-spline least square	0.23	0.20

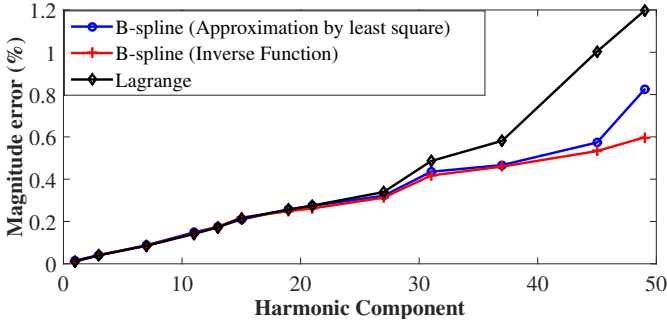


**Figure 9** Harmonic components error (ramp variation).

### 4.2 Signals with interharmonics

In the second case, the results are obtained from the signals composed by interharmonics and an off-nominal frequency of 60.03 Hz. The interharmonic magnitude is 10% of the fundamental, and the frequencies of these components are 82.5 Hz and 145 Hz. The estimated interharmonic magnitude and frequency are presented in Table 3, in which the largest frequency error is obtained by the B-spline with pre-filter using least square approximation. The error is 0.05 and 0.08 Hz, considering the interharmonics with 82.5 and 145 Hz, respectively. Comparing the magnitude, the largest error was obtained estimating the interharmonic with the frequency of 82.5 Hz using the re-sampling based on Lagrange. Figure 11 shows the harmonic relative errors obtained by re-sampling methods, where the errors maintain the value under 1.2%. The largest error is obtained by B-spline with the least square approximation in the pre-filter. The maximum value is approximately 1.1% for 49th order harmonic. The B-spline with inverse function pre-filter and Lagrange remain below 1%. The MRE and the MSE obtained from harmonic estimation are presented in Table 4. The results for all methods showed high accuracy. The larger MRE errors are obtained by Lagrange and B-spline with approximation least square pre-filter. The larger MSE error is obtained by B-spline applying

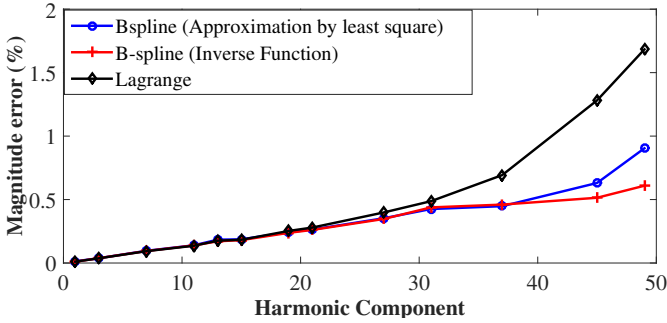


**Figure 10** Harmonic components error (sinusoidal variation).

**Table 3** Results of the interharmonics estimation with frequencies of 82.5 and 145 Hz.

	Mag./Freq.	Mag./Freq.
Real	0.1000/82.5	0.1000/145
Lagrange	0.1002/82.46	0.1000/144.93
B-spline Inverse F.	0.1001/82.46	0.1000/144.93
B-spline least square	0.0999/82.45	0.1001/144.92

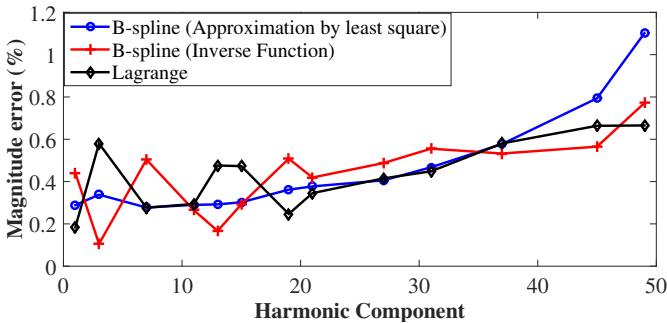


**Figure 11** Harmonic Components error considering signals with interharmonic components.

least square pre-filter, and the smaller is obtained by B-spline using inverse function pre-filter.

### 4.3 Signals with interharmonics and frequency deviation

In this case, a signal with the harmonics and interharmonics components is considered. The interharmonic frequencies are 82.5 Hz and 145 Hz. The fundamental component is considered with a frequency equal to 60.1 Hz. The value of the harmonic relative errors is shown in Figure 12, where it can be noted that the lowest value is obtained with B-spline using an inverse function pre-filter. Considering all re-sampling methods, the errors have considerable accuracy in this scenario. The magnitude of interharmonic is presented in

**Table 4** MRE and MSE values considering signals with interharmonics.

Re-sampling Method	MRE	MSE
Lagrange	0.44	0.50
B-spline Inverse F.	0.36	0.38
B-spline least square	0.44	0.51

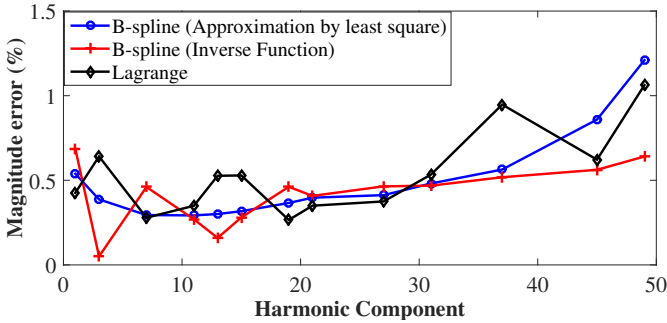


**Figure 12** Harmonic components errors considering a frequency deviation.

**Table 5** Results of the interharmonic with frequencies of 82.5 and 145 Hz.

	Mag./Freq.	Mag./Freq.
Real	0.1000/82.5	0.1000/145
Lagrange	0.1000/82.35	0.0999/144.75
B-spline Inverse F.	0.1000/82.36	0.1000/144.76
B-spline least square	0.0999/82.37	0.1001/144.76

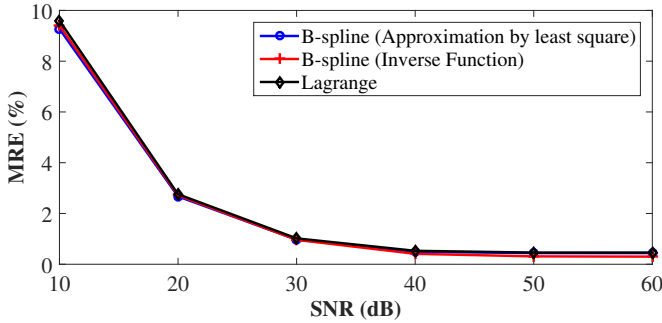
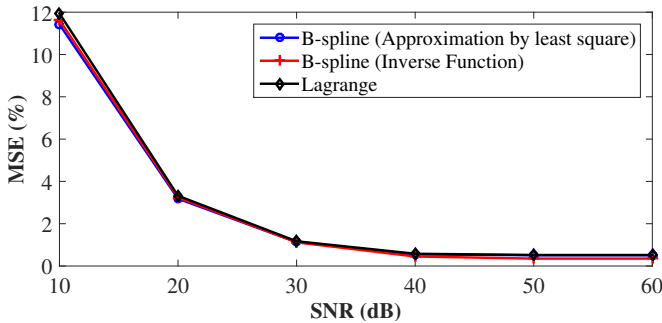
Table 5, in which the maximum frequencies errors are 0.15 and 0.25 Hz obtained by re-sampling with Lagrange function, considering the interharmonics with the frequency equal 82.5 and 145 Hz, respectively. The largest magnitude error is obtained by B-spline with the approximation pre-filter. The MRE and MSE are presented in Table 6, in which all re-sampling methods present high accuracy. Considering the results, the highest error is obtained by re-sampling with the Lagrange function and the lowest one is obtained by the B-spline with inverse function pre-filter.

#### 4.4 Estimation with different noise

In this subsection, the re-sampling methods are applied in a scenario with the SNR values considered in the range of 10 and 60 dB. In this case, the signals are composed of interharmonic components with frequencies equal to 82.5 and 145 Hz, and the fundamental frequency is equal to 60.3 Hz. The MRE and MSE of the three re-sampling methods are presented in Figure 13 and Figure 14. According to the results, we noted that the method presents high performance for noise equal to or larger than 20 dB, where the MRE and MSE values remained under 3 and 4%, respectively. The smallest and largest errors are presented in Figure 15 (a) and (b), in which the three re-sampling methods

**Table 6** MRE and MSE obtained considering a signal with interharmonic and frequency deviation.

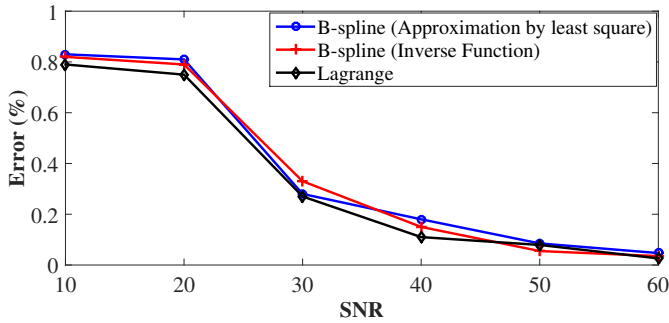
Re-sampling Method	MRE	MSE
Lagrange	0.48	0.53
B-spline Inverse F.	0.33	0.36
B-spline least square	0.45	0.52

**Figure 13** MRE obtained in the harmonic estimation.**Figure 14** MSE obtained in the harmonic estimation.

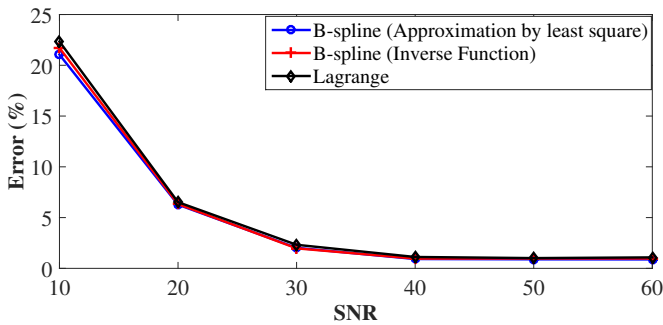
present analog results. Considering Figure 15 (a), the values are maintained under 1% for all SNR values. Analyzing Figure 15 (b), the errors are largest in the range of 10 and 20 dB. Considering the SNR larger than or equal to 30 dB the largest error is smaller than 2.5%.

#### 4.5 Components estimation for different B-spline pre-filter order

This subsection considers different pre-filter orders for the two B-spline pre-filter functions. The signal is composed of two interharmonics, with frequencies equal to 85 Hz and 145 Hz and magnitude equal to 10% of the fundamental. In this case, the fundamental frequency is equal to 60.3 Hz. The MRE and MSE obtained by the B-spline pre-filter based on inverse function and least square



(a)



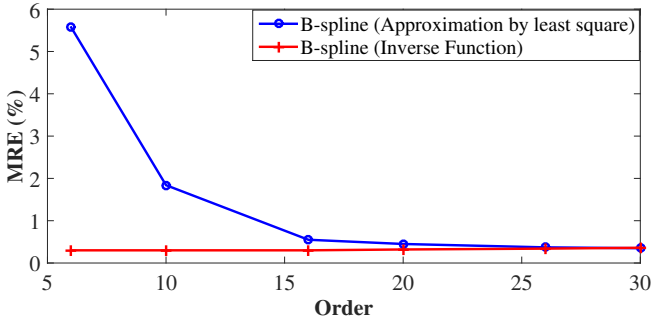
(b)

**Figure 15** (a) smallest, and (b) largest error obtained by different noise.

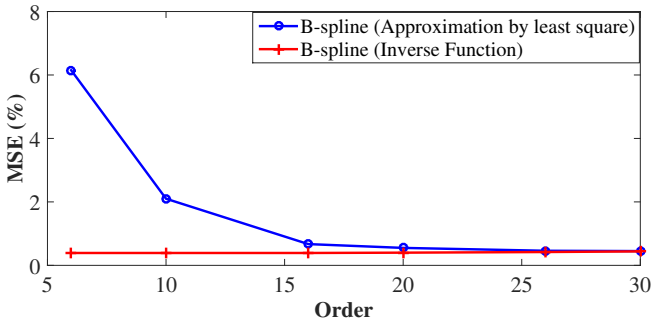
are shown in Figure 16 (a) and (b). The results show that the B-spline pre-filter based on least square, results in more significant errors for low orders, while the B-spline based on the inverse function remains constant for all pre-filter orders. The smallest and largest errors are shown in Figure 16 (a) and (b), where the B-spline with pre-filter based on the least square presents smallest values, remaining under 0.35% in high orders. However, the largest errors are obtained in low orders. The B-spline based on the inverse function, on the other hand, presents low errors for all orders.

## 5 Discussion and Conclusion

This work presents a method to estimate harmonics and interharmonics in signals with asynchronous sampling, composed of components with small magnitude and non-multiple frequency resolution. The method is applied in real-time to avoid storing the estimated frequency samples. At first, two re-sampling methods are applied to mitigate the spectral leakage provided by asynchronous sampling. One of the methods consists of the B-spline function and the second consists of the Lagrange function. The re-sampling method



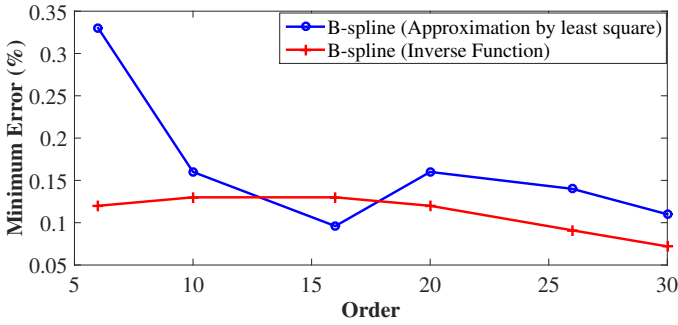
(a)



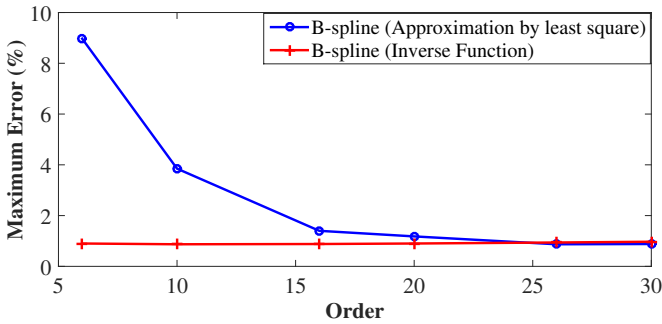
(b)

**Figure 16** (a) MRE and (b) MSE obtained in the harmonic estimation.

based on the B-spline function was implemented with two different pre-filter functions. The first pre-filter is based on the inverse function and the second is based on the least square approximation. The results showed that the re-sampling methods contributed to improving the harmonic estimation due to avoiding leakage. However, they do not avoid the leakage caused by interharmonics with non-multiple frequency resolution. Thus, to improve the interharmonic estimation, the IpDFT was proposed. The results showed that the harmonic and interharmonic components are satisfactorily estimated using B-spline and Lagrange re-sampling methods, and the IpDFT. However, the B-spline using the inverse function pre-filter provided the best performance in all scenarios considered in this work. The re-sampling based on B-spline with the inverse function pre-filter and IpDFT showed robustness in frequency variation scenario and for different SNR values, and presented high accuracy to estimate interharmonic with non-integer multiple of the frequency resolution.



(a)



(b)

**Figure 17** (a) Smallest error and (b) largest errors obtained in the harmonic estimation.

## 6 Acknowledgments

The authors would like the Federal University of Lavras, Federal University of Juiz de Fora, State University of Campinas, Polytechnic School at University of São Paulo, CAPES, CNPQ and FAPEMIG - Finance Code APQ-01379-22.

## 7 Declarations

### 7.1 Competing interests

The authors declare that they have no competing interests.

### 7.2 Authors' contributions

- Conception and design of the study: H. L. M. Monteiro and C. A. Duque.
- Acquisition of data: H. L. M. Monteiro, L. A. F. Rodrigues.
- Analysis and/or interpretation of data: H. L. M. Monteiro, C. A. Duque.

- Drafting the manuscript: H. L. M. Monteiro, L. F. A. Rodrigues, D.D. Ferreira, T. W. Cabral, M. O. Mostaro, F. M. Dias, R. A. Ribeiro, C. A. Duque.
- Revising of the version of the manuscript to be published: H. L. M. Monteiro, C. A. Duque, M. A. A. Lima, D. D. Ferreira. L. R. M. Silva.

## References

- [1] Melo, Igor D., and Matheus P. Antunes. "A novel approach for harmonic responsibility assessment based on an optimization model." *Electrical Engineering* 104.5 (2022).
- [2] F. G. Montoya, et al. "Analysis of power flow under non-sinusoidal conditions in the presence of harmonics and interharmonics using geometric algebra." *International Journal of Electrical Power & Energy Systems* 111 (2019).
- [3] H. Ardi, A. Ajami, and M. Sabahi. "Analysis and implementation of a novel three input DC-DC boost converter for sustainable energy applications." *International Transactions on Electrical Energy Systems* 29.4 (2019).
- [4] W. R. Oliveira, L. F. Anesio Filho, and J. Cormane. "A contribution for the measuring process of harmonics and interharmonics in electrical power systems with photovoltaic sources." *International Journal of Electrical Power & Energy Systems* 104 (2019).
- [5] Pramanik, Meghabriti, Aurobinda Routray, and Pabitra Mitra. "A two-stage adaptive symmetric-strong-tracking square-root cubature Kalman filter for harmonics and interharmonics estimation." *Electric Power Systems Research* 210 (2022).
- [6] M. Bollen, et al. "Standards for supraharmonics (2 to 150 kHz)." *IEEE Electromagnetic Compatibility Magazine* 3.1 (2014): 114-119.
- [7] T. M. Mendes, et al. "Supraharmonic analysis by filter bank and compressive sensing." *Electric Power Systems Research* 169 (2019): 105-114.
- [8] T. M. Mendes, et al. "Supraharmonic analysis by filter bank and compressive sensing." *Electric Power Systems Research* 169 (2019).
- [9] S. Lodetti, et al. "A Robust Wavelet-based Hybrid Method for the Simultaneous Measurement of Harmonic and Supraharmonic Distortion." *IEEE Transactions on Instrumentation and Measurement* (2020).
- [10] V. Khokhlov, et al. "Comparison of Measurement Methods for the Frequency Range 2 - 150 kHz (Supraharmonics) Based on the Present Standards Framework." *IEEE Access* 8 (2020).

- [11] S. K. Mitra, *Digital Signal Processing - A computer based Approach*, 3rd ed., Ed. New York: McGraw-Hill, (2006).
- [12] C. Altintasi, et al. "Power system harmonic and interharmonic estimation using Vortex Search Algorithm." *Electric Power Systems Research* 182 (2020).
- [13] A. Testa, D. Gallo, and R. Langella. "On the processing of harmonics and interharmonics: Using Hanning window in standard framework." *IEEE Transactions on Power Delivery* 19.1 (2004).
- [14] A. Testa, et al. "Interharmonics: Theory and modeling." *IEEE Transactions on Power Delivery* 22.4 (2007).
- [15] V. Ravindran, et al. "Time-varying interharmonics in different types of grid-tied PV inverter systems." *IEEE Transactions on Power Delivery* 35.2 (2019).
- [16] A. Sangwongwanich, and F. Blaabjerg. "Mitigation of interharmonics in PV systems with maximum power point tracking modification." *IEEE Transactions on Power Electronics* 34.9 (2019).
- [17] A. Sangwongwanich, et al. "Analysis and modeling of interharmonics from grid-connected photovoltaic systems." *IEEE Transactions on Power Electronics* 33.10 (2018).
- [18] Chen, Lei, et al. "An interharmonic phasor and frequency estimator for subsynchronous oscillation identification and monitoring." *IEEE Transactions on Instrumentation and Measurement* 68.6 (2018).
- [19] V. Ravindran, S. K. Rönnerberg, and M. H. J. Bollen. "Interharmonics in PV systems: a review of analysis and estimation methods; considerations for selection of an apt method." *IET Renewable Power Generation* 13.12 (2019): 2023-2032.
- [20] E. Santos, et al. "ESPRIT associated with filter bank for power-line harmonics, sub-harmonics and interharmonics parameters estimation." *International Journal of Electrical Power & Energy Systems* 118 (2020): 105731.
- [21] P. D. Achlerkar, S. R. Samantaray, and M. Sabarimalai Manikandan. "Variational mode decomposition and decision tree based detection and classification of power quality disturbances in grid-connected distributed generation system." *IEEE Transactions on Smart Grid* 9.4 (2016): 3122-3132.

- [22] Z. Sun, et al. "Multi-interharmonic spectrum separation and measurement under asynchronous sampling condition." *IEEE Transactions on Instrumentation and Measurement* 65.8 (2016): 1902-1912.
- [23] K. Wang, H. Wen, and G. Li. "Accurate Frequency Estimation by Using Three Points Interpolated DFT Based on Rectangular Window." *IEEE Transactions on Industrial Informatics* (2020).
- [24] A. K. Singh, and B. C. Pal. "Rate of change of frequency estimation for power systems using interpolated DFT and Kalman filter." *IEEE Transactions on Power Systems* 34.4 (2019): 2509-2517.
- [25] G. Frigo, A. Derviškadić, and Mario Paolone. "Reduced leakage synchrophasor estimation: Hilbert transform plus interpolated DFT." *IEEE Transactions on Instrumentation and Measurement* 68.10 (2018): 3468-3483.
- [26] A. Derviškadić, P. Romano, and M. Paolone. "Iterative-interpolated DFT for synchrophasor estimation: A single algorithm for P-and M-class compliant PMUs." *IEEE Transactions on Instrumentation and Measurement* 67.3 (2017): 547-558.
- [27] Y. Wang, W. Wei, and J. Xiang. "Multipoint interpolated DFT for sine waves in short records with DC components." *Signal Processing* 131 (2017): 161-170.
- [28] D. Petrinovic,. "Causal cubic splines: Formulations, interpolation properties and implementations." *IEEE Transactions on Signal Processing* 56.11 (2008): 5442-5453.
- [29] G. W. Chang, and Cheng-I. Chen. "An accurate time-domain procedure for harmonics and interharmonics detection." *IEEE Transactions on Power Delivery* 25.3 (2009): 1787-1795.
- [30] D. Borkowski, and A. Bien. "Improvement of accuracy of power system spectral analysis by coherent resampling." *IEEE Transactions on Power Delivery* 24.3 (2009): 1004-1013.
- [31] C. Moler, (2004), *Numerical Computing with MatLab*, [Online], Available: <http://www.mathworks.com/moler/chapters.html>.
- [32] Monteiro, Henrique LM, et al. "A DFT-based method for estimating interharmonics in wind power generation." *IET Smart Grid* (2022).
- [33] Monteiro, Henrique Luis Moreira, et al. "Comparison of interpolation methods in time and frequency domain for the estimation of harmonics and interharmonics according to IEC standard." 2014 16th International

Conference on Harmonics and Quality of Power (ICHQP). IEEE, (2014).

- [34] International Electrotechnical Commission: IEC 61000-4-7, Testing and measurement techniques - General guide on harmonics and interharmonics measurements and instrumentation, for power supply systems and equipment connected thereto, (2002).
- [35] Z. Liu, J. Himmel, and K. W. Bonfig. "Improved processing of harmonics and interharmonics by time-domain averaging." *IEEE transactions on power delivery* 20.4 (2005).
- [36] I. J. Schoenberg. "Contributions to the problem of approximation of equidistant data by analytic functions." *IJ Schoenberg Selected Papers*. Birkhäuser, Boston, MA, (1988).
- [37] M. Unser. "Splines: A perfect fit for signal and image processing." *IEEE Signal processing magazine* 16.6 (1999): 22-38.
- [38] P. F. Ribeiro, C. A. Duque, P. M. da Silveira, A. S. Cerqueira, *Power Systems Signal Processing for Smart Grids*, New York, Wiley, (2014), p. 232.